ACS Partner Journal

Journal of the American Society for Mass Spectrometry

pubs.acs.org/jasms

Research Article

Influence of N Terminus Amino Acid on Peptide Cleavage in Solution through Diketopiperazine Formation

Zhi-chao Zhang, David A. Hales,* and David E. Clemmer*

Cite This: *J. Am. Soc. Mass Spectrom.* 2022, 33, 1368−1376

Read Online

ACCESS | Metrics & More | Article Recommendations | Supporting Information

ABSTRACT: Diketopiperazine (DKP) formation is an important degradation pathway for peptides and proteins. It can occur during synthesis and storage in either solution or the solid state. The kinetics of peptide cleavage through DKP formation have been analyzed for the model peptides Xaa^1-Pro^2-Gly$_4$-Lys^7 [Xaa = Gln, Glu, Lys, Ser, Phe, Trp, Tyr, Cha (β-cyclohexylalanine), Aib (α-aminoisobutyric acid), Gly, and Val] at multiple elevated temperatures in ethanol with ion mobility spectrometry−mass spectrometry (IMS−MS). When Xaa is an amino acid with a charged or polar side chain, degradation is relatively fast. When Xaa is an amino acid with a nonpolar alkyl side chain, the peptide is relatively stable. For these peptides, a bulky group on the α carbon speeds up dissociation, but the kinetic effects vary in a complicated manner for bulky groups on the β or γ carbon. Peptides where Xaa has a nonpolar aromatic side chain show moderate dissociation rates. The stability of these peptides is a result of multiple factors. The reaction rate is enhanced by (1) the stabilization of the late transition state through the interaction of an aromatic ring with the nascent DKP ring or lowering the activation energy of nucleophilic attack intermediate state through polar or charged residues and (2) the preference of the *cis* proline bond favored by the aromatic N-terminus. The number of unseen intermediates and transition state thermodynamic values are derived for each peptide by modeling the kinetics data. Most of the transition states are entropically favored ($\Delta S^{\ddagger} \sim -5$ to $+31$ J·mol^{-1}·K^{-1}), and all are enthalpically disfavored ($\Delta H^{\ddagger} \sim 93$ to 109 kJ·mol^{-1}). The Gibbs free energy of activation is similar for all of the peptides studied here ($\Delta G^{\ddagger} \sim 90-99$ kJ·mol^{-1}).

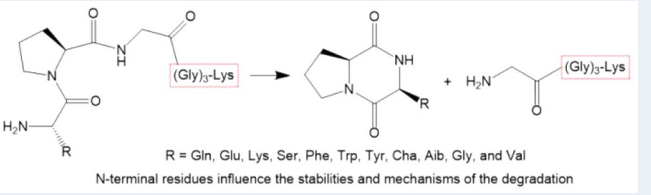

INTRODUCTION

Diketopiperazine (2,5-dioxopiperazine, DKP) formation is a spontaneous intramolecular aminolysis reaction that forms a DKP dipeptide from the first two amino acids of the parent peptide, leaving the remainder of the truncated sequence as a second fragment (Scheme 1). This happens most often when a peptide contains penultimate proline and has an unprotected N terminus.[1−4] The mechanism requires the amino group in the N terminal residue to come into close proximity with the carbonyl group between the second and third residues.[5] In order for this to happen, a *cis* penultimate proline is required; therefore, *trans* → *cis* isomerization of the Xaa^1-Pro^2 peptide bond usually occurs prior to the dissociation.

DKP formation is a common process that happens during the storage of peptides as well as during peptide synthesis.[3,6,7] This process can also be found within the human body, generating a wide range of biologically active dipeptides such as cyclo (His-Pro).[8,9] These dipeptides are important in terms of neurophysiological function in tissues and body fluids.[8,10] In addition, a variety of phosphorylated peptides are found to be strongly associated with cancer and serve as potential targets for drug development against cancer.[11] Of particular interest is that a majority of these peptides contain a penultimate proline and thus are susceptible to DKP formation. Therefore, understanding the DKP formation is of critical importance. Because this is a Focus issue for Peter Armentrout, we cannot resist mentioning the b_2 product ion, on which many pioneering studies have been done.[12−15] In previous work with substance P, we compared formation of the b_2 ion by gas-phase activation to DKP formation in solution and discussed the energetics of those two processes.[16] We do not pursue that further in this paper.

Ion mobility spectrometry−mass spectrometry (IMS−MS) has been receiving increasing attention due to its advantage of resolving isomers with different collisional cross sections (CCS).[17] Previous study on the peptide bradykinin (Arg^1-Pro^2-Pro^3-Gly^4-Phe^5-Ser^6-Pro^7-Phe^8-Arg^9) shows a slow configurationally coupled protonation process.[18] A study on neuropeptide substance P (Arg^1-Pro^2-Lys^3-Pro^4-Gln^5-Gln^6-Phe^7-Phe^8-Gly^9-Leu^{10}-Met^{11}) captured the sequential cleavage event of the Pro^2-Lys^3 bond followed by the cleavage of the Pro^4-Gln^5 bond.[19] A study that focused on the solvent effect on DKP formation implies that the local environment where the peptide resides can generate a great impact on its stability,[20]

Special Issue: Focus: Gas-Phase Ion Chemistry

Received: February 8, 2022
Revised: May 3, 2022
Accepted: May 3, 2022
Published: May 16, 2022

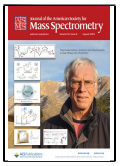

Scheme 1. Cleavage reaction of Pro^2-Gly^3 by DKP formation with Xaa^1-Pro^2 in the *cis* configuration

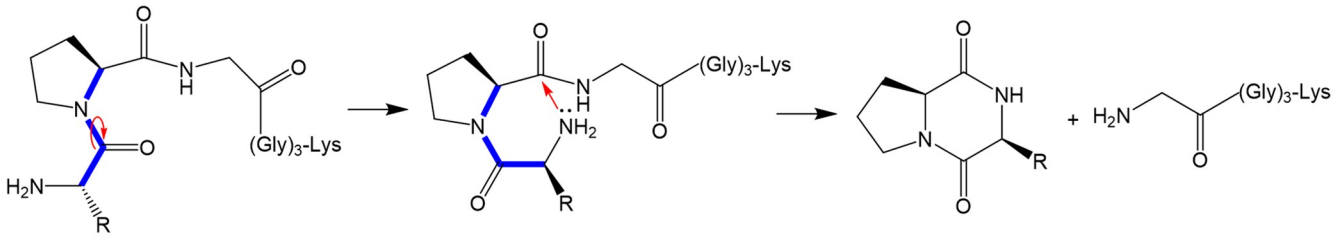

which is analogous to enzymatic processes.[21] Recently, we studied the influence of peptide length on peptide dissociation structural changes and mechanisms.[22] In this study, we utilize IMS combined with MS to systematically study the influence of the N-terminal residue on stability with a series of model peptides Xaa^1-Pro^2-Gly_4-Lys^7. A few reports studied the N-terminal effect on DKP formation rate but were confined to short peptides.[5,23,24] In these studies, the potential interaction between the C- and N-terminus cannot be excluded, making it impossible to gain insight into the effect on dissociation rate induced only by the N-terminus amino acid. In this study, longer linkers are used in each model peptide, and explanations are proposed for understanding the different stabilities of peptides with various N-terminal residues. Potential dissociation pathways are derived, and transition-state thermodynamic values behind the reaction are extracted. Higher numbers of unseen intermediates are found in stable peptides. For peptides with the same number of intermediates, activation energy determines the relative stability. Gibbs free energies of activation are mainly regulated by enthalpy. We have measured the variation in rates for this process in water, methanol, ethanol, and *n*-propanol.[20] We have chosen to conduct all the work described here in ethanol, as in another earlier study,[22] because the intermediate rates in that solvent allow for practical monitoring of the reaction kinetics.

EXPERIMENTAL SECTION

Sample Preparation and Electrospray Ionization (ESI) Conditions. Peptide Xaa^1-Pro^2-Gly_4-Lys^7 analogues were synthesized using an Applied Biosystems 433A Peptide Synthesizer (Applied Biosystems, Foster City, CA) based on a well-documented Fmoc (9-fluorenylmethoxycarbonyl) solid-phase peptide synthesis procedure.[25] All solvents involved in the synthesis including DMF, DCM, MeOH, and diethyl ether were of the highest purity. Liquid chromatography was used to purify the desired peptides. The purified peptides were dissolved into pure ethanol to make 1 mM stock solutions, which were stored at −20 °C. Stock solutions were diluted to 20 μM in ethanol with 1% acetic acid (by volume), followed by electrospray from a Nano-ESI (Triversa nanomate, Advion Biosciences, Ithica, NY) auto sampler. Throughout the experiment, the ESI voltage was kept at 1.2 kV.

Instrumentation and Kinetics Experiment. During the kinetics experiment, samples are incubated in separate vials independently in a water bath at multiple defined temperatures. The dissociation experiments were conducted in triplicate. The samples were monitored periodically with a home-built 2-m drift tube instrument coupled with a time-of-flight mass spectrometer as shown in Figure S1. Detailed descriptions of the instrument and IMS−MS theory can be found elsewhere.[26−34] Briefly, ions generated by ESI are collected and stored in the ion funnel represented as F1 in Figure S1.[35] Packets of ions are pulsed into the drift tube periodically. The drift tube is filled with ∼3 Torr of 298 K He buffer gas. While the ions migrate through the two drift tube segments D1 and D2, they are separated based on their gas-phase mobility under the influence of a weak uniform electric field (∼10 V·cm^{-1}). As ions exit the drift tube, they are ejected orthogonally into a time-of-flight mass analyzer to measure their m/z value.[36] CCS are derived according to the following equation[28]

$$\Omega = \frac{(18\pi)^{1/2}}{16}\frac{ze}{(k_bT)^{1/2}}\left[\frac{1}{m_I}+\frac{1}{m_B}\right]^{1/2}\frac{t_DE}{L}\frac{760}{P}\frac{T}{273.2}\frac{1}{N} \quad (1)$$

where the relevant terms are drift time (t_D), ion charge (ze), Boltzmann's constant (k_b), mass of the ion (m_I), mass of the buffer gas (m_B), temperature (T), electric field value (E), drift tube length (L), pressure of buffer gas (P), and buffer gas neutral number density (N).

In some studies,[18,19] we are able to detect the singly charged cDKP along with the other doubly charged fragment, while in other systems, it is difficult to detect the singly charged cDKP.[22] We believe that in this study the lack of singly charged cDKP is due to instrument discrimination. If we changed the settings to detect both fragment ions, we would give up the ability to detect the precursor ions. Therefore, in this study, we focused on the doubly charged G_4K and precursor ions.

RESULTS AND DISCUSSION

Mass Spectral Data for Xaa^1-Pro^2-Gly_4-Lys^7 Peptide Dissociation. Figure 1 shows DKP degradation mass spectra of the peptide Glu^1-Pro^2-Gly_4-Lys^7 at 75 °C. At 0 min, the mass spectrum shows one peak at m/z = 301, which corresponds to the $[EPG_4K+2H]^{2+}$ ion. At 30 min, the degradation yields the doubly charged fragment ion $[G_4K+2H]^{2+}$. As the incubation time progresses to 45 min, the $[G_4K+2H]^{2+}$ fragment ion grows in abundance while the intact peptide $[EPG_4K+2H]^{2+}$ ion decreases in abundance. By 130 min, the degradation is completed, and only the $[G_4K+2H]^{2+}$ fragment ion remains in the spectrum. The dissociation half-life is ∼46 min. Dissociation mass spectra for peptides with Xaa = Cha (β-cyclohexylalanine), Val, Trp, Phe, Tyr, Lys, Ser, and Gly are shown in Figure S2. All these dissociations follow the DKP formation mechanism illustrated in Scheme 1.

Figure 2 shows the dissociation half-lives for a set of Xaa^1-Pro^2-Gly_4-Lys^7 analogues (Xaa = Cha, Val, Trp, Phe, Tyr, Lys, Ser, and Gly) at 75, 70, and 65 °C. It turns out that varying the amino acid residue at the N-terminus, next to the penultimate proline, generates an obvious effect on the peptide's dissociation rate. The general trend is that when the N-terminal residue is a polar or charged amino acid (Gln, Glu,

https://doi.org/10.1021/jasms.2c00037
J. Am. Soc. Mass Spectrom. 2022, 33, 1368−1376

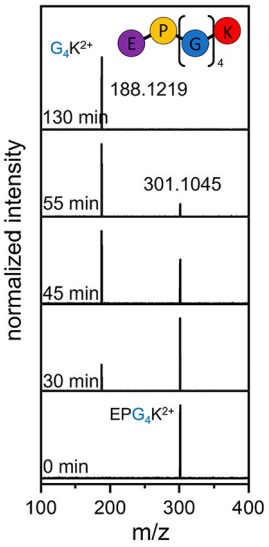

Figure 1. Dissociation mass spectra of peptide Glu[1]-Pro[2]-Gly$_4$-Lys[7] in ethanol with 1% acetic acid (by volume) at 75 °C. Self-cleavage of Pro[2]-Gly[3] bond happens with a half-life of 46 min.

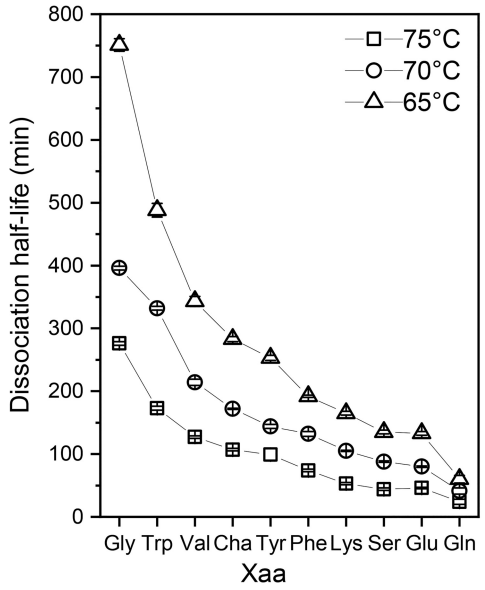

Figure 2. Dissociation half-lives of peptides Xaa[1]-Pro[2]-Gly$_4$-Lys[7] (Xaa = Gly, Trp, Val, Cha, Tyr, Phe, Lys, Ser, Glu, and Gln) at 75, 70, and 65 °C in ethanol with 1% acetic acid (by volume).

Ser, Lys), the dissociation has relatively fast kinetics, and when the N-terminal residue is nonpolar (Gly, Val) the dissociation rate is slow. When the N-terminal amino acid contains an aromatic group (Phe, Tyr), the dissociation rate is between the rate of the charged/polar amino acids and the nonpolar amino acids. One special case is when Xaa is Trp: although Trp contains an aromatic residue, the dissociation rate of Trp[1]-Pro[2]-Gly$_4$-Lys[7] is close to peptides Val[1]-Pro[2]-Gly$_4$-Lys[7] and Gly[1]-Pro[2]-Gly$_4$-Lys[7]. The dissociation half-lives are listed in Table 1.

Determination of Penultimate Proline Configuration. Alanine substitution experiments were performed in order to determine the configuration of penultimate proline in these peptides. Unlike proline that can exist in either the *cis* or *trans* configuration, alanine only allows for the *trans* isomer.

Table 1. Summary of Half-Lives of Peptides Xaa[1]-Pro[2]-Gly$_4$-Lys[7] (Xaa= Gly, Trp, Val, Cha, Tyr, Phe, Lys, Ser, Glu, and Gln)

	dissociation half-life[a] (min)		
Xaa	75 °C	70 °C	65 °C
Gly	276 ± 3	396 ± 3	751 ± 10
Trp	173 ± 3	332 ± 3	488 ± 8
Val	127 ± 2	214 ± 5	343 ± 4
Cha	107 ± 2	172 ± 1	283 ± 4
Tyr	99 ± 10	144 ± 3	253 ± 2
Phe	74 ± 2	132 ± 4	192 ± 3
Lys	53 ± 2	105 ± 1	165 ± 3
Ser	44 ± 2	88 ± 1	135 ± 3
Glu	46 ± 1	80 ± 1	133 ± 3
Gln	24 ± 4	41 ± 5	60 ± 6

[a]The reported dissociation half-lives are the averaged value and standard deviation from triplicate measurements.

Therefore, after substitution, if the structure does not change, we label the proline configuration as *trans*. Otherwise, we label the proline configuration as *cis*. Figure 3 shows the CCS distribution profiles of doubly charged Xaa[1]-Pro[2]-Gly$_4$-Lys[7] (Xaa = Glu, Ser, Tyr, and Gly) and their alanine substituted analogues (analogous data for other peptides are shown in Figure S3). All of the CCS values for alanine-substituted peptides are corrected according to the intrinsic size parameter difference between alanine and proline as described previously.[37] The CCS distribution of Ser[1]-Pro[2]-Gly$_4$-Lys[7] shows no overlap with its Pro[2]-Ala substituted analogue, indicating that Ser[1]-Pro[2]-Gly$_4$-Lys[7] contains exclusively *cis*-Pro[2]. This aligns with its relatively fast dissociation rate among the peptides in this study. In contrast, other peptides show peaks that align with their alanine-substituted analogues, suggesting the existence of *trans*-Pro[2] in these peptides.

CCS Distribution Profiles of Precursor Ions during Dissociation. Figure 4 shows the CCS distribution change of peptide Xaa[1]-Pro[2]-Gly$_4$-Lys[7] (Xaa = Glu, Tyr, and Gly) (similar figures for Xaa = Lys, Cha, Val, Trp, and Phe are shown in Figure S4). The phenomenon of decreasing FWHM was observed during dissociation in a previous study.[22] This is likely because several gas-phase conformers are formed from the *trans* solution conformer but cannot be resolved by IMS. As the peptide undergoes *trans* → *cis* isomerization of the Xaa[1]-Pro[2] peptide bond, the decrease in abundance of the *trans* isomer results in the narrowing of the mobility peaks of these conformers. The mobility peak centers of Xaa[1]-Pro[2]-Gly$_4$-Lys[7] (Xaa = Trp, Val, and Gly) shift to a higher CCS value, which suggests a configuration change of proline from *trans* to *cis* during dissociation. In contrast, the peak center of other peptides remains in the same position. This is probably because the *trans* and *cis* isomers are too close in CCS value to be separated by this IMS instrument. The Xaa[1]-Pro[2]-Gly$_4$-Lys[7] peptides that dissociate most slowly (Xaa = Trp, Val, and Gly) are also those where the *cis* and *trans* isomers can be differentiated, so this larger difference in cross section may indicate a more significant—and slower—conformational change.

Understanding the Stability of Peptides with Different N-Terminus Residues. In order to evaluate the influence on dissociation rate induced by the benzyl group on the N-terminus, the hydrophobically similar but nonaromatic amino acid Cha is used to replace Phe as a control. As shown in

https://doi.org/10.1021/jasms.2c00037
J. Am. Soc. Mass Spectrom. 2022, 33, 1368−1376

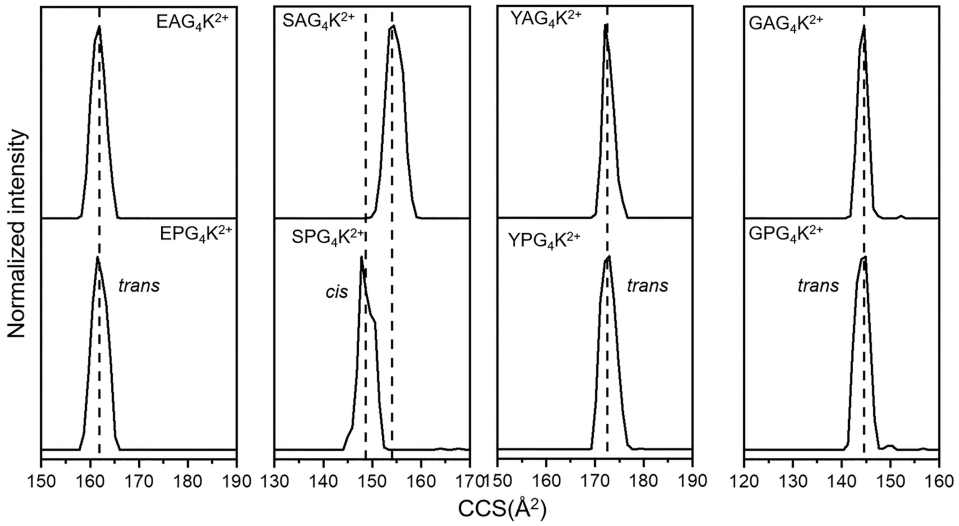

Figure 3. CCS distribution for peptide Xaa[1]-Pro[2]-Gly$_4$-Lys[7] (Xaa = Glu, Ser, Tyr, and Gly) and their Pro[2] to Ala substituted peptide. Distributions are acquired in ethanol with 1% acetic acid (by volume). CCS distributions of Ala substituted peptides are corrected with intrinsic size parameter between Pro and Ala residues.

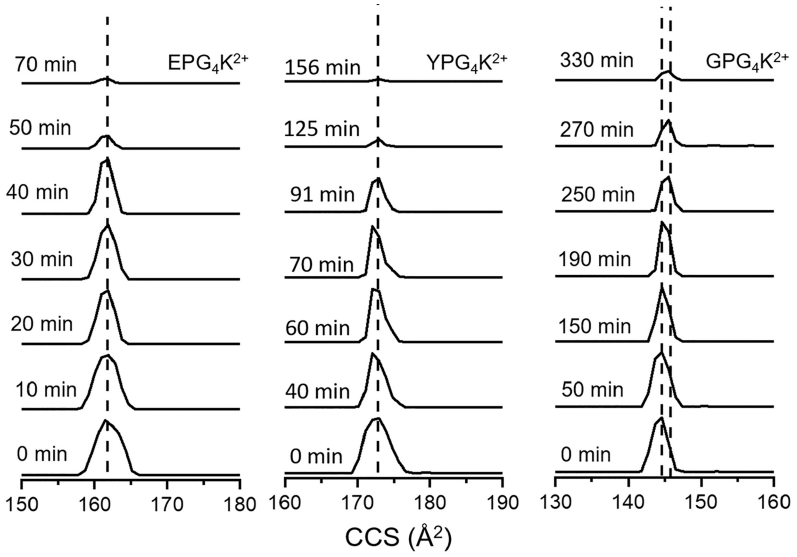

Figure 4. CCS distribution for doubly charged peptide Xaa[1]-Pro[2]-Gly$_4$-Lys[7] (Xaa = Glu, Tyr, and Gly) at different dissociation times.

Figure 2, replacing Phe with Cha makes the peptide more stable. This suggests the aromaticity of the benzyl group located on the N-terminal side of the proline residue favors the dissociation kinetics, which means it must lower the transition-state energy. This is likely due to two reasons. First, the aromatic moiety enhances the conformational stability of the transition state. It is well-documented that when there is an aromatic group in the cyclic dipeptide the DKP ring will stay in a boat-shaped conformation with the aromatic group folded over the DKP ring.[38,39] The intramolecular dipole−induced dipole interaction between the DKP ring and the aromatic π electrons makes this structure energetically favored.[39] We propose that the transition state resembles the product (a "late" transition state), and the free energy barrier to reach this transition state is lowered by the interaction between the benzyl group and the DKP ring as it forms. Second, the interaction between the aromatic residue and proline promotes the formation of *cis* amide bonds,[40−52] the prolyl that favors DKP formation. Another example of this is the stability of the peptide with Tyr as the N-terminal residue. Previous research shows that the Tyr-Pro pair exhibits higher *cis* amide bond composition than Phe-Pro,[45,47,53−57] but we found the peptide Tyr[1]-Pro[2]-Gly$_4$-Lys[7] is more stable than the peptide Phe[1]-Pro[2]-Gly$_4$-Lys7 under our experimental conditions. Therefore, in this case, the hydroxyl-substituted ring in Tyr must be less effective at lowering the energy of the transition state than is the phenyl in Phe. Of particular interest is the slow dissociation rate of the peptide Trp[1]-Pro[2]-Gly$_4$-Lys[7] compared to the peptide Tyr[1]-Pro[2]-Gly$_4$-Lys[7] and Phe[1]-Pro[2]-Gly$_4$-Lys[7]. The CCS value of Trp[1]-Pro[2]-Gly$_4$-Lys[7] is 164.1 ± 2 Å^2, while Tyr[1]-Pro[2]-Gly$_4$-Lys[7] and Phe[1]-Pro[2]-Gly$_4$-Lys[7] are 172.9 ± 3 and 169.4 ± 2 Å^2, respectively. In spite of the larger side chain on Trp compared to Tyr and Phe, Trp[1]-Pro[2]-Gly$_4$-Lys[7] is a more compact structure than Tyr[1]-Pro[2]-Gly$_4$-Lys[7] and Phe[1]-Pro[2]-Gly$_4$-Lys[7]. This is likely due to intramolecular interactions that stabilize the *trans* isomer, slowing its conversion to the *cis*

https://doi.org/10.1021/jasms.2c00037
J. Am. Soc. Mass Spectrom. 2022, 33, 1368−1376

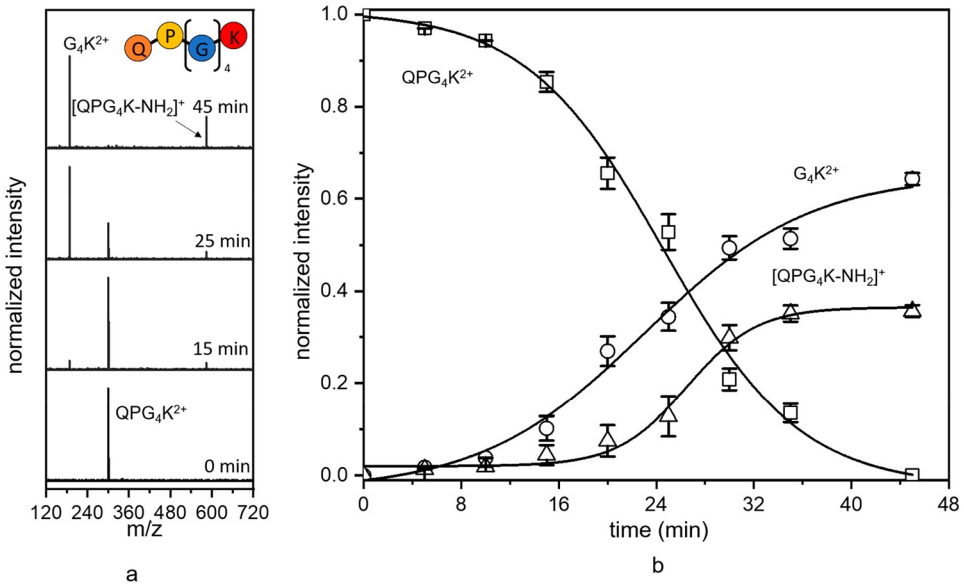

Figure 5. Dissociation mass spectra (a) and relative abundance plot (b) of peptide Gln^1-Pro^2-Gly_4-Lys^7 in ethanol with 1% acetic acid (by volume) at 75 °C. DKP formation by self-cleavage of Pro^2–Gly^3 bond as well as formation of pyroglutamate $[QPG_4K - NH_3]^+$ happens during the incubation. The dissociation half-life is ~24 min.

conformer and subsequent dissociation. In addition, the different electron-withdrawing ability between indole and benzene rings can contribute to the difference in dissociation rate.

The rapid dissociation of peptides with charged or uncharged polar side chains (Xaa = Lys, Glu, and Ser) likely results from the stability of the transition state. The nucleophilic attack of the amino group on the carbonyl group to form the DKP ring involves electrostatic attraction between atoms with partial charges, so a charged or polar side chain can lower the energy of the transition state during dissociation, thus favoring the degradation.

It is interesting that when the N-terminal amino acid is Gln the peptide degrades through two parallel pathways as shown in Figure 5. Figure 5a shows mass spectra of the peptide Gln^1-Pro^2-Gly_4-Lys^7's dissociation at 75 °C. During the incubation, two new peaks appear. One corresponds to formation of DKP product with m/z = 188. The other peak is at m/z = 583, which corresponds to loss of NH_3 from $[QPG_4K+2H]^{2+}$. The m/z = 583 product is a pyroglutamate moiety that is produced by the cyclization of Gln.[58−60] Scheme 2 illustrates a simple mechanism of pyroglutamate formation through nucleophilic attack[59] by the N-terminal amino group on the carbonyl carbon of the Gln side chain. The same reaction can happen with glutamate at the N terminus but with a slower rate as shown in a previous study.[61] (No pyroglutamate formation is detected with peptide Glu^1-Pro^2-Gly_4-Lys^7 under our experimental conditions.) Figure 5b shows the normalized intensity of each product during the dissociation as a function of time. It turns out that the DKP formation and pyroglutamate formation begin around the same incubation time but DKP formation mechanism is the major dissociation pathway.

Scheme 2. Pyroglutamate formation reaction of peptide Gln^1-Pro^2-Gly_4-Lys^7 with N-terminal Gln

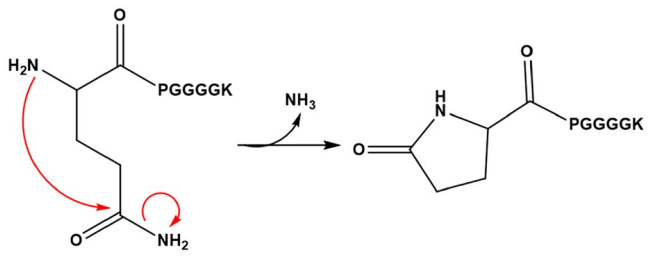

Peptides with nonpolar amino acids as the N-terminal residue are more stable compared to other peptides: the dissociation half-lives at 75 °C for the peptide Gly^1-Pro^2-Gly_4-Lys^7 and Val^1-Pro^2-Gly_4-Lys^7 are 276 and 127 min, respectively (Figure 2). This indicates that there is no interaction induced by Gly and Val that speeds up the dissociation kinetics as compared to peptides with either aromatic or polar N terminal residues. Previous research shows that increasing the bulkiness of the substituent in intramolecular organic reactions enhances the cyclization rate.[62] Accordingly, DKP formation is faster when Xaa is Val, with its isopropyl side chain, than when Xaa is Gly.

In order to achieve a deeper understanding of the steric bulk effect, we ran dissociation of Xaa^1-Pro^2-Gly_4-Lys^7 (Xaa = Aib, Ile, Ala, and Leu) at 75 °C with identical solution conditions (Figure 2S). It turns out that increasing the bulkiness of the α-carbon in the N-terminal residue speeds up the dissociation rate dramatically: Aib^1-Pro^2-Gly_4-Lys7 degrades completely in 8 min at 75 °C, as shown in Figure S5. By replacing Val with Ile and introducing a methyl group two carbons away from the α-carbon, the dissociation rate increases slightly compared to Val^1-Pro^2-Gly_4-Lys^7 and the half-life decreases by just 7 min. This means the bulkiness on the γ-carbon has only a small impact on DKP formation. Both Ala^1-Pro^2-Gly_4-Lys^7 and Leu^1-Pro^2-Gly_4-Lys^7 have a dissociation half-life ~50 min. The dissociation rates are roughly twice as fast as those of Val^1-Pro^2-Gly_4-Lys^7 and Ile^1-Pro^2-Gly_4-Lys^7, which is similar to previous studies.[63−66] It turns out that bulkiness at the β-carbon has a complex effect on DKP dissociation rate.

Characterizing Potential Dissociation Pathways. For each peptide, a number of different mechanisms are proposed

https://doi.org/10.1021/jasms.2c00037
J. Am. Soc. Mass Spectrom. 2022, 33, 1368−1376

to fit with the experimental kinetics data, and the sums of squares of fitting residuals are compared in order to understand the dynamics behind the degradation. A detailed description of the fitting method is provided elsewhere.[67] We first fit the data with the simplest pathway: direct formation of G_4K from EPG_4K, as shown by the following reaction:

$$[EPG_4K + 2H]^{2+} \rightarrow [G_4K + 2H]^{2+} + cEP \quad (2)$$

In Figure 6, the dashed lines represent the best fitting curve of this model with experimental kinetics data for each

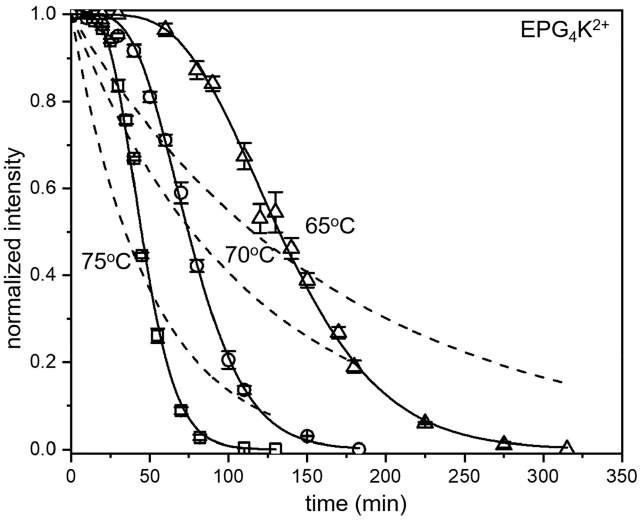

Figure 6. Normalized abundances of doubly charged peptide $[EPG_4K + 2H]^{2+}$ as incubation progresses in ethanol. Hollow rectangles, circles, and triangles represent experimental data at 75, 70, and 65 °C. Kinetic fits from two models are shown: model 1 (dashed lines) and the best-fitting model (solid lines). Details can be found in Table 2.

temperature. Obviously, this model fails to capture the general trend of the dissociation. We then compare 13 more mechanisms for this dissociation. Table 2 shows the sums of squares of the fitting residuals for each candidate mechanism. It shows that the best representation of the Glu^1-Pro^2-Gly_4-Lys^7 dissociation data (ΣRSS at a minimum) is found with six intermediates. This fit appears in Figure 6 (solid curves). Analogous figures of the total sum of squares of the residuals and sequential models for dissociation kinetics of Xaa^1-Pro^2-Gly_4-Lys^7 when Xaa = Aib, Ser, Lys, Phe, Tyr, Cha, Val, Trp, and Gly are shown in Tables S1–S9 (ΣRSS) and Figures S6–S14 (fits). For each peptide, over 10 mechanisms are compared. The number of unseen intermediates involved in the dissociation pathway of peptide Xaa^1-Pro^2-Gly_4-Lys^7 are six, seven, and eight, respectively, for Xaa = Aib, Ser, Lys, while Xaa = Phe, Tyr, Cha, Val, Trp, and Gly all have 17 unseen intermediates. These unseen intermediates are derived from the best fitting model, though not detected by the IMS–MS instrument. The results show peptides with fast dissociation kinetics tend to have fewer intermediates during the induction period compared to peptides that have slow dissociation kinetics.

Transition-State Thermodynamics. Measurements of the kinetics data at different solution temperatures were used to derive Arrhenius plots based on eq 3

$$\ln(k) = \frac{-E_a}{R} \cdot \frac{1}{T} + \ln(A) \quad (3)$$

where E_a and A represent activation energy and pre-exponential factor, respectively (Figures S15–S24). We are able to derive enthalpy, entropy, and Gibbs free energy according to eqs 4–6 based on transition-state theory

$$\Delta H^{\ddagger} = E_a + RT \quad (4)$$

$$A = \frac{ek_BT}{h} e^{\Delta S^{\ddagger}/R} \quad (5)$$

$$\Delta G^{\ddagger} = \Delta H^{\ddagger} - T\Delta S^{\ddagger} \quad (6)$$

where h is Planck's constant, k_B is Boltzmann's constant, R is the gas constant, T is temperature of the reaction, and e is Euler's number. Table 3 shows the step-by-step thermochemistry values for the dissociation process. Peptides with N-terminal residues such as Phe, Tyr, Cha, Val, Trp, and Gly have the same number of intermediates, so the transition-state Gibbs free energy barrier heights reflect their relative dissociation rates: the peptide with the fastest dissociation kinetics has the lowest transition state Gibbs free energy barrier. In addition, it is worth noting that all but two of the dissociation processes are entropically favored and have a loose transition state for sequential steps leading toward degradation. The entropy of activation is slightly negative for Xaa = Phe and Tyr. As discussed above, these aromatic side chains are believed to position themselves over the DKP ring as it forms in order to lower the barrier to that reaction. These $\Delta S^{\ddagger}$ values indicate that the aromatic groups in Xaa = Phe and Tyr must be positioned more precisely in the late transition state than the side chains of other Xaa^1-Pro^2-Gly_4-Lys^7 peptides. By replacing Phe and Tyr with hydrophobically similar but nonaromatic amino acid Cha, a positive entropy of activation is found, indicating the importance of benzyl in stabilizing the transition state. For all of the peptides in this study, the transition state Gibbs free energies of activation are mainly determined enthalpically.

SUMMARY AND CONCLUSION

All the peptides we have studied in the Xaa^1-Pro^2-Gly_4-Lys^7 family undergo fragmentation through a mechanism that cleaves off Xaa^1-Pro^2 as a DKP. This is the sole fragmentation mechanism for all except Gln^1-Pro^2-Gly_4-Lys^7, in which a pyroglutamate mechanism happens in parallel with DKP formation, making the dissociation kinetics the fastest among all the peptides in the study. Our data show that the type of N-terminal amino acid in Xaa^1-Pro^2-Gly_4-Lys^7 has a significant impact on the peptide's relative susceptibility to this dissociation process: the dissociation is fastest when Xaa is a charged or polar amino acid and slowest when Xaa is a nonpolar amino acid. Temperature-dependent kinetic analysis indicated that that there are sequential unimolecular mechanisms for the dissociation, from which transition state enthalpies, entropies, and free energies are derived. Interactions known to occur within precursor peptides and dipeptides in DKP form were proposed to affect the characteristics of either a transition state or a late transition state, thus rationalizing most of the variations in these peptides' dissociation rates. The stability of the peptide is related to both number of transition state intermediates and Gibbs free energy barrier.

https://doi.org/10.1021/jasms.2c00037
J. Am. Soc. Mass Spectrom. 2022, 33, 1368–1376

Table 2. Modeled Reaction Mechanisms Compared with Experimental Kinetics Data of the Glu[1]-Pro[2]-Gly$_4$-Lys[7] Dissociation in Ethanol

Model No.	Model reaction mechanism	Sum of residuals squared
1	$[EPG_4K+2H]^{2+} \rightarrow [G_4K+2H]^{2+}$	1.16
2	$[EPG_4K+2H]^{2+} \rightarrow i_1 \rightarrow [G_4K+2H]^{2+}$	0.548
3	$[EPG_4K+2H]^{2+} \rightarrow i_1 \rightarrow [G_4K+2H]^{2+}$	0.524
4	$[EPG_4K+2H]^{2+} \rightarrow i_1 \rightarrow [G_4K+2H]^{2+}$; $i_1 \rightarrow i_2 \rightarrow [G_4K+2H]^{2+}$	1.16
5	$[EPG_4K+2H]^{2+} \rightarrow i_1 \rightarrow i_2 \rightarrow [G_4K+2H]^{2+}$	0.34
6	$[EPG_4K+2H]^{2+} \rightarrow i_1 \rightarrow i_2 \rightarrow [G_4K+2H]^{2+}$; $i_1 \rightarrow i_3 \rightarrow [G_4K+2H]^{2+}$	0.565
7	$[EPG_4K+2H]^{2+} \rightarrow i_1 \rightarrow i_2 \rightarrow i_3 \rightarrow [G_4K+2H]^{2+}$	0.21
8	$[EPG_4K+2H]^{2+} \rightarrow i_1 \rightarrow i_3 \rightarrow [G_4K+2H]^{2+}$; $i_1 \rightarrow i_2 \rightarrow [G_4K+2H]^{2+}$	0.256
9	$[EPG_4K+2H]^{2+} \rightarrow i_1 \rightarrow \ldots \rightarrow i_4 \rightarrow [G_4K+2H]^{2+}$	0.108
10	$[EPG_4K+2H]^{2+} \rightarrow i_1 \rightarrow \ldots \rightarrow i_5 \rightarrow [G_4K+2H]^{2+}$	0.0417
11	$[EPG_4K+2H]^{2+} \rightarrow i_1 \rightarrow \ldots \rightarrow i_6 \rightarrow [G_4K+2H]^{2+}$	0.0327
12	$[EPG_4K+2H]^{2+} \rightarrow i_1 \rightarrow \ldots \rightarrow i_6 \rightarrow [G_4K+2H]^{2+}$; $i_1 \rightarrow i_7 \rightarrow [G_4K+2H]^{2+}$	0.245
13	$[EPG_4K+2H]^{2+} \rightarrow i_1 \rightarrow \ldots \rightarrow i_7 \rightarrow [G_4K+2H]^{2+}$	0.0354
14	$[EPG_4K+2H]^{2+} \rightarrow i_1 \rightarrow \ldots \rightarrow i_8 \rightarrow [G_4K+2H]^{2+}$	0.0452

Table 3. Summary of Transition-State Thermodynamic Data of Peptide Xaa[1]-Pro[2]-Gly$_4$-Lys[7] (Xaa= Aib, Glu, Ser, Lys, Phe, Tyr, Cha, Val, Trp, and Gly)

Xaa	n^a	$\Delta G^{\ddagger}$ (kJ·mol^{-1})	$\Delta H^{\ddagger}$ (kJ·mol^{-1})	$\Delta S^{\ddagger}$ (J·mol^{-1}·K^{-1})	E_a (kJ·mol^{-1})
Aib	6	90.4 ± 1.2	97.8 ± 0.9	24.8 ± 2.7	95.3 ± 0.8
Glu	6	97.7 ± 2.5	106.9 ± 1.9	30.7 ± 5.3	104.4 ± 1.9
Ser	7	97.0 ± 1.1	102.4 ± 0.8	18.1 ± 2.3	99.9 ± 0.8
Lys	8	97.9 ± 2.5	108.5 ± 2.4	35.4 ± 1.7	106.0 ± 2.4
Phe	17	94.6 ± 0.9	93.2 ± 0.7	−4.7 ± 2.0	90.7 ± 0.7
Tyr	17	95.4 ± 0.7	94.5 ± 0.6	−3.1 ± 1.4	92.0 ± 0.6
Cha	17	95.3 ± 2.0	98.0 ± 2.0	9.1 ± 1.9	95.5 ± 2.0
Val	17	96.8 ± 1.5	99.3 ± 1.1	8.5 ± 3.2	96.9 ± 1.1
Trp	17	98.4 ± 0.5	104.4 ± 0.4	20.3 ± 1.0	101.9 ± 0.4
Gly	17	99.3 ± 2.1	105.0 ± 1.6	19.1 ± 4.6	102.5 ± 1.6

[a]n represents the number of unseen intermediates derived from the best-fitting model.

■ ASSOCIATED CONTENT

Supporting Information

The Supporting Information is available free of charge at https://pubs.acs.org/doi/10.1021/jasms.2c00037.

2-m IMS−MS instrument diagram (Figure S1); dissociation mass spectra of peptide Xaa[1]-Pro[2]-Gly$_4$-Lys[7] (Xaa = Cha, Val, Trp, Phe, Tyr, Lys, Ser, and Gly) (Figures S2); CCS distribution for peptide Xaa[1]-Pro[2]-Gly$_4$-Lys[7] (Xaa = Cha, Phe, Lys, Val, and Trp) and their Pro[2] to Ala substituted peptide (Figure S3); CCS distribution for peptide Xaa[1]-Pro[2]-Gly$_4$-Lys[7] (Xaa = Cha, Phe, Lys, Val, and Trp) at different dissociation times (Figure S4); dissociation mass spectra of peptide (Aib)-PG$_4$K (Figure S5); sequential models for the dissociation kinetics of Xaa[1]-Pro[2]-Gly$_4$-Lys[7] (Xaa = Aib, Cha, Val, Trp, Phe, Tyr, Lys, Ser, and Gly) (Figures S6−14); Arrhenius plot for mechanism mentioned in the main text (Figures S15−24); modeled reaction mechanisms

https://doi.org/10.1021/jasms.2c00037
J. Am. Soc. Mass Spectrom. 2022, 33, 1368−1376

compared with experimental kinetics data of peptides in the main text (Table S1−S9) (PDF)

AUTHOR INFORMATION

Corresponding Authors

David A. Hales − *Department of Chemistry, Hendrix College, Conway, Arkansas 72032, United States*; Email: hales@hendrix.edu

David E. Clemmer − *Department of Chemistry, Indiana University, Bloomington, Indiana 47405, United States*; orcid.org/0000-0003-4039-1360; Email: clemmer@indiana.edu

Author

Zhi-chao Zhang − *Department of Chemistry, Indiana University, Bloomington, Indiana 47405, United States*

Complete contact information is available at: https://pubs.acs.org/10.1021/jasms.2c00037

Notes

The authors declare no competing financial interest.

ACKNOWLEDGMENTS

This work is supported in part by funds from the National Institutes of Health grant 5R01GM121751-0 (D.E.C.), the Robert and Marjorie Mann Graduate Research Fellowship from Indiana University (Z.Z.), and Faculty Project/Leave Grant #S0077 from Hendrix College (D.A.H.). We thank Dr. Fa Zhang for help with peptide synthesis and Hua Pan and Navneet Sahota for experimental assistance.

REFERENCES

(1) Pedroso, E.; Grandas, A.; de las Heras, X.; Eritja, R.; Giralt, E. Diketopiperazine formation in solid phase peptide synthesis using p-alkoxybenzyl ester resins and Fmoc-amino acids. *Tetrahedron Lett.* **1986**, *27* (6), 743−746.

(2) Rydon, H.; Smith, P. 702. Polypeptides. Part IV. The self-condensation of the esters of some peptides of glycine and proline. *J. Chem. Soc.* **1956**, 3642−3650.

(3) Battersby, J.; Hancock, W.; Canova-Davis, E.; Oeswein, J.; O'onnor, B. Diketopiperazine formation and N-terminal degradation in recombinant human growth hormone. *Int. J. Pept. Protein Res.* **1994**, *44* (3), 215−222.

(4) Beyermann, M.; Bienert, M.; Niedrich, H.; Carpino, L. A.; Sadat-Aalaee, D. Rapid continuous peptide synthesis via FMOC amino acid chloride coupling and 4-(aminomethyl) piperidine deblocking. *J. Org. Chem.* **1990**, *55* (2), 721−728.

(5) Capasso, S.; Vergara, A.; Mazzarella, L. Mechanism of 2, 5-dioxopiperazine formation. *J. Am. Chem. Soc.* **1998**, *120* (9), 1990−1995.

(6) Kertscher, U.; Bienert, M.; Krause, E.; Sepetov, N. F.; Mehlis, B. Spontaneous chemical degradation of substance P in the solid phase and in solution. *Int. J. Pept. Protein Res.* **1993**, *41* (3), 207−211.

(7) Steinberg, S.; Bada, J. L. Diketopiperazine formation during investigations of amino acid racemization in dipeptides. *Science* **1981**, *213* (4507), 544−545.

(8) Møss, J.; Bundgaard, H. Kinetics and mechanism of the facile cyclization of histidyl-prolineamide to cyclo (His-Pro) in aqueous solution and the competitive influence of human plasma. *J. Pharm. Pharmacol* **2011**, *42* (1), 7−12.

(9) Miyashita, K.; Murakami, M.; Yamada, M.; Iriuchijima, T.; Mori, M. Histidyl-proline diketopiperazine. Novel formation that does not originate from thyrotropin-releasing hormone. *J. Biol. Chem.* **1993**, *268* (28), 20863−20865.

(10) Ienaga, K.; Nakamura, K.; Kurohashi, M.; Nakanishi, T.; Ichii, T. Hydroxyproline-containing diketopiperazines inducing drought resistance in rice. *Phytochem. Lett.* **1990**, *29* (1), 35−39.

(11) Cobbold, M.; De La Peña, H.; Norris, A.; Polefrone, J. M.; Qian, J.; English, A. M.; Cummings, K. L.; Penny, S.; Turner, J. E.; Cottine, J. MHC class I−associated phosphopeptides are the targets of memory-like immunity in leukemia. *Sci. Transl. Med.* **2013**, *5* (203), 203ra125−203ra125.

(12) Farrugia, J. M.; Taverner, T.; Richard, A. Side-chain involvement in the fragmentation reactions of the protonated methyl esters of histidine and its peptides. *Int. J. Mass Spectrom.* **2001**, *209* (2−3), 99−112.

(13) Perkins, B. R.; Chamot-Rooke, J.; Yoon, S. H.; Gucinski, A. C.; Somogyi, Á.; Wysocki, V. H. Evidence of diketopiperazine and oxazolone structures for HA b2+ ion. *J. Am. Chem. Soc.* **2009**, *131* (48), 17528−17529.

(14) Armentrout, P.; Clark, A. A. The simplest b2+ ion: determining its structure from its energetics by a direct comparison of the threshold collision-induced dissociation of protonated oxazolone and diketopiperazine. *Int. J. Mass Spectrom.* **2012**, *316*, 182−191.

(15) Nelson, C. R.; Abutokaikah, M. T.; Harrison, A. G.; Bythell, B. J. Proton mobility in b2 ion formation and fragmentation reactions of histidine-containing peptides. *J. Am. Soc. Mass. Spectrom* **2016**, *27* (3), 487−497.

(16) Conant, C. R.; Fuller, D. R.; Zhang, Z.; Woodall, D. W.; Russell, D. H.; Clemmer, D. E. Substance P in the gas phase: conformational changes and dissociations induced by collisional activation in a drift tube. *J. Am. Soc. Mass. Spectrom* **2019**, *30* (6), 932−945.

(17) Sahota, N.; AbuSalim, D. I.; Wang, M. L.; Brown, C. J.; Zhang, Z.; El-Baba, T. J.; Cook, S. P.; Clemmer, D. E. A microdroplet-accelerated Biginelli reaction: mechanisms and separation of isomers using IMS-MS. *Chem. Sci.* **2019**, *10* (18), 4822−4827.

(18) Fuller, D. R.; Conant, C. R.; El-Baba, T. J.; Brown, C. J.; Woodall, D. W.; Russell, D. H.; Clemmer, D. E. Conformationally regulated peptide bond cleavage in bradykinin. *J. Am. Chem. Soc.* **2018**, *140* (30), 9357−9360.

(19) Conant, C. R.; Fuller, D. R.; El-Baba, T. J.; Zhang, Z.; Russell, D. H.; Clemmer, D. E. Substance P in solution: trans-to-cis configurational changes of penultimate prolines initiate non-enzymatic peptide bond cleavages. *J. Am. Soc. Mass. Spectrom* **2019**, *30* (6), 919−931.

(20) Zhang, Z.-c.; Raab, S. A.; Hales, D. A.; Clemmer, D. E. Influence of Solvents upon Diketopiperazine Formation of FPG_8K. *J. Phys. Chem. B* **2021**, *125* (11), 2952−2959.

(21) Frackenpohl, J.; Arvidsson, P. I.; Schreiber, J. V.; Seebach, D. The outstanding biological stability of β-and γ-peptides toward proteolytic enzymes: an in vitro investigation with fifteen peptidases. *ChemBioChem.* **2001**, *2* (6), 445−455.

(22) Zhang, Z.; Conant, C. R.; El-Baba, T. J.; Raab, S. A.; Fuller, D. R.; Hales, D. A.; Clemmer, D. E. Diketopiperazine Formation from FPG_nK (n = 1−9) Peptides: Rates of Structural Rearrangements and Mechanisms. *J. Phys. Chem. B* **2021**, *125* (29), 8107−8116.

(23) Capasso, S.; Mazzarella, L. Solvent effects on diketopiperazine formation from N-terminal peptide residues. *J. Chem. Soc., Perkin Trans.* **1999**, *2* (2), 329−332.

(24) Fuller, D. R.; Conant, C. R.; El-Baba, T. J.; Zhang, Z.; Molloy, K. R.; Zhang, C. S.; Hales, D. A.; Clemmer, D. E. Monitoring the stabilities of a mixture of peptides by mass-spectrometry-based techniques. *Eur. J. Mass Spectrom* **2019**, *25* (1), 73−81.

(25) Coin, I.; Beyermann, M.; Bienert, M. Solid-phase peptide synthesis: from standard procedures to the synthesis of difficult sequences. *Nat. Protoc* **2007**, *2* (12), 3247.

(26) Koeniger, S. L.; Merenbloom, S. I.; Sevugarajan, S.; Clemmer, D. E. Transfer of structural elements from compact to extended states in unsolvated ubiquitin. *J. Am. Chem. Soc.* **2006**, *128* (35), 11713−11719.

(27) Mesleh, M.; Hunter, J.; Shvartsburg, A.; Schatz, G. C.; Jarrold, M. Structural information from ion mobility measurements: effects of

the long-range potential. *J. Phys. Chem.* **1996**, *100* (40), 16082−16086.
(28) Mason, E. A.; McDaniel, E. W. *Transport Properties of Ions in Gases*; John Wiley & Sons: Hoboken, NJ, 1988.
(29) Revercomb, H.; Mason, E. A. Theory of plasma chromatography/gaseous electrophoresis. Review. *Anal. Chem.* **1975**, *47* (7), 970−983.
(30) Wyttenbach, T.; von Helden, G.; Batka, J. J.; Carlat, D.; Bowers, M. T. Effect of the long-range potential on ion mobility measurements. *J. Am. Soc. Mass Spectrom.* **1997**, *8* (3), 275−282.
(31) Bohrer, B. C.; Merenbloom, S. I.; Koeniger, S. L.; Hilderbrand, A. E.; Clemmer, D. E. Biomolecule analysis by ion mobility spectrometry. *Annu. Rev. Anal. Chem.* **2008**, *1*, 293−327.
(32) McLean, J. A.; Ruotolo, B. T.; Gillig, K. J.; Russell, D. H. Ion mobility−mass spectrometry: a new paradigm for proteomics. *Int. J. Mass spectrom* **2005**, *240* (3), 301−315.
(33) Kanu, A. B.; Dwivedi, P.; Tam, M.; Matz, L.; Hill, H. H. Ion mobility−mass spectrometry. *J. Mass Spectrom* **2008**, *43* (1), 1−22.
(34) Merenbloom, S. I.; Koeniger, S. L.; Valentine, S. J.; Plasencia, M. D.; Clemmer, D. E. IMS−IMS and IMS−IMS−IMS/MS for separating peptide and protein fragment ions. *Anal. Chem.* **2006**, *78* (8), 2802−2809.
(35) Tang, K.; Shvartsburg, A. A.; Lee, H.-N.; Prior, D. C.; Buschbach, M. A.; Li, F.; Tolmachev, A. V.; Anderson, G. A.; Smith, R. D. High-Sensitivity Ion Mobility Spectrometry/Mass Spectrometry Using Electrodynamic Ion Funnel Interfaces. *Anal. Chem.* **2005**, *77*, 3330−3339.
(36) Hoaglund, C. S.; Valentine, S. J.; Sporleder, C. R.; Reilly, J. P.; Clemmer, D. E. Three-dimensional ion mobility/TOFMS analysis of electrosprayed biomolecules. *Anal. Chem.* **1998**, *70* (11), 2236−2242.
(37) Glover, M. S.; Dilger, J. M.; Acton, M. D.; Arnold, R. J.; Radivojac, P.; Clemmer, D. E. Examining the influence of phosphorylation on peptide ion structure by ion mobility spectrometry-mass spectrometry. *J. Am. Soc. Mass. Spectrom* **2016**, *27* (5), 786−794.
(38) Buděšínský, M.; Symerský, J.; Ječný, J.; Van Hecke, J.; Hosten, N.; Anteunis, M.; Borremans, F. Cyclo (l-propyl-l-N-methylphenylalanyl) Conformation in solution and in the crystal. *Int. J. Pept. Protein Res.* **1992**, *39* (2), 123−130.
(39) Liwo, A.; Ciarkowski, J. Origin of the ring-ring interaction in cyclic dipeptides incorporating an aromatic amino acid. *Tetrahedron Lett.* **1985**, *26* (15), 1873−1876.
(40) Grathwohl, C.; Wüthrich, K. The X-Pro peptide bond as an NMR probe for conformational studies of flexible linear peptides. *Biopolymers* **1976**, *15* (10), 2025−2041.
(41) Montelione, G.; Arnold, E.; Meinwald, Y.; Stimson, E.; Denton, J.; Huang, S.; Clardy, J.; Scheraga, H. Chain-folding initiation structures in ribonuclease A: conformational analysis of trans-Ac-Asn-Pro-Tyr-NHMe and trans-Ac-Tyr-Pro-Asn-NHMe in water and in the solid state. *J. Am. Chem. Soc.* **1984**, *106* (25), 7959−7969.
(42) Dyson, H. J.; Rance, M.; Houghten, R. A.; Lerner, R. A.; Wright, P. E. Folding of immunogenic peptide fragments of proteins in water solution: I. Sequence requirements for the formation of a reverse turn. *J. Mol. Biol.* **1988**, *201* (1), 161−200.
(43) Stewart, D. E.; Sarkar, A.; Wampler, J. E. Occurrence and role of cis peptide bonds in protein structures. *J. Mol. Biol.* **1990**, *214* (1), 253−260.
(44) Poznański, J.; Ejchart, A.; Wierzchowski, K.; Ciurak, M. 1H-and 13C-NMR investigations on cis−trans isomerization of proline peptide bonds and conformation of aromatic side chains in H-Trp-(Pro) n-Tyr-OH peptides. *Biopolymers* **1993**, *33* (5), 781−795.
(45) Yao, J.; Feher, V. A.; Espejo, B. F.; Reymond, M. T.; Wright, P. E.; Dyson, H. J. Stabilization of a type VI turn in a family of linear peptides in water solution. *J. Mol. Biol.* **1994**, *243* (4), 736−753.
(46) Kemmink, J.; Creighton, T. E. The physical properties of local interactions of tyrosine residues in peptides and unfolded proteins. *J. Mol. Biol.* **1995**, *245* (3), 251−260.
(47) Reimer, U.; Scherer, G.; Drewello, M.; Kruber, S.; Schutkowski, M.; Fischer, G. Side-chain effects on peptidyl-prolyl cis/trans isomerisation. *J. Mol. Biol.* **1998**, *279* (2), 449−460.
(48) Wu, W. J.; Raleigh, D. P. Local control of peptide conformation: stabilization of cis proline peptide bonds by aromatic proline interactions. *Biopolymers* **1998**, *45* (5), 381−394.
(49) Pal, D.; Chakrabarti, P. Cis peptide bonds in proteins: residues involved, their conformations, interactions and locations. *J. Mol. Biol.* **1999**, *294* (1), 271−288.
(50) Thomas, K. M.; Naduthambi, D.; Zondlo, N. J. Electronic control of amide cis−trans isomerism via the aromatic−prolyl interaction. *J. Am. Chem. Soc.* **2006**, *128* (7), 2216−2217.
(51) Brown, A. M.; Zondlo, N. J. A propensity scale for type II polyproline helices (PPII): aromatic amino acids in proline-rich sequences strongly disfavor PPII due to proline−aromatic interactions. *Biochemistry* **2012**, *51* (25), 5041−5051.
(52) Zondlo, N. J. Aromatic−proline interactions: electronically tunable CH/π interactions. *Acc. Chem. Res.* **2013**, *46* (4), 1039−1049.
(53) Grathwohl, C.; Wüthrich, K. The X-Pro peptide bond as an NMR probe for conformational studies of flexible linear peptides. *Biopolymers: Original Research on Biomolecules* **1976**, *15* (10), 2025−2041.
(54) Forbes, C. C.; Beatty, A. M.; Smith, B. D. Using pentafluorophenyl as a Lewis acid to stabilize a cis secondary amide conformation. *Org. Lett.* **2001**, *3* (22), 3595−3598.
(55) Yamasaki, R.; Tanatani, A.; Azumaya, I.; Saito, S.; Yamaguchi, K.; Kagechika, H. Amide conformational switching induced by protonation of aromatic substituent. *Org. Lett.* **2003**, *5* (8), 1265−1267.
(56) Wu, W. J.; Raleigh, D. P. Local control of peptide conformation: stabilization of cis proline peptide bonds by aromatic proline interactions. *Biopolymers: Original Research on Biomolecules* **1998**, *45* (5), 381−394.
(57) Halab, L.; Lubell, W. D. Effect of sequence on peptide geometry in 5-tert-butylprolyl type VI β-turn mimics. *J. Am. Chem. Soc.* **2002**, *124* (11), 2474−2484.
(58) Rehder, D. S.; Dillon, T. M.; Pipes, G. D.; Bondarenko, P. V. Reversed-phase liquid chromatography/mass spectrometry analysis of reduced monoclonal antibodies in pharmaceutics. *J. Chromatogr. A* **2006**, *1102* (1−2), 164−175.
(59) Baglioni, C. The role of pyrrolidone carboxylic acid in the initiation of immunoglobulin peptide chains. *Biochem. Biophys. Res. Commun.* **1970**, *38* (2), 212−219.
(60) Orlowska, A.; Witowska, E.; Izdebski, J. Sequence dependence in the formation of pyroglutamyl peptides in solid phase peptide synthesis. *Int. J. Pept. Protein Res.* **1987**, *30* (1), 141−144.
(61) Schilling, S.; Wasternack, C.; Demuth, H.-U. Glutaminyl cyclases from animals and plants: a case of functionally convergent protein evolution. *Biol. Chem.* **2008**, *389* (8), 983−991.
(62) Borchardt, R. T.; Cohen, L. A. Stereopopulation control. III. Facilitation of intramolecular conjugate addition of the carboxyl group. *J. Am. Chem. Soc.* **1972**, *94* (26), 9175−9182.
(63) Goolcharran, C.; Borchardt, R. T. Kinetics of diketopiperazine formation using model peptides. *J. Pharm. Sci.* **1998**, *87* (3), 283−288.
(64) Bruice, T. C.; Bradbury, W. C. The gem effect. II. The influence of 3-mono-and 3, 3-disubstitution on the rates of solvolysis of mono-p-bromophenyl glutarate. *J. Am. Chem. Soc.* **1965**, *87* (21), 4846−4850.
(65) Higuchi, T.; Eberson, L.; McRae, J. D. Acid anhydride-free acid equilibria in water in some substituted succinic acid systems and their interaction with aniline. *J. Am. Chem. Soc.* **1967**, *89* (12), 3001−3004.
(66) Borchardt, R. T.; Cohen, L. A. Stereopopulation control. II. Rate enhancement of intramolecular nucleophilic displacement. *J. Am. Chem. Soc.* **1972**, *94* (26), 9166−9174.
(67) El-Baba, T. J.; Kim, D.; Rogers, D. B.; Khan, F. A.; Hales, D. A.; Russell, D. H.; Clemmer, D. E. Long-Lived Intermediates in a Cooperative Two-State Folding Transition. *J. Phys. Chem. B* **2016**, *120* (47), 12040−12046.

https://doi.org/10.1021/jasms.2c00037
J. Am. Soc. Mass Spectrom. 2022, 33, 1368−1376